SUPPLEMENTARY MATERIAL 1: SAMPLES, DETAILED METHODS AND SUPPORTING PLOTS

S1.1. Samples

S1.1.1. Rock descriptions, selected field photos and photomicrographs

MD19-22: Quartz metamicrodiorite sampled at Hanlon Park, West Baltimore, in creek bed of Gwynns Run, immediately upstream (north) of where the creek passes under Gwynns Falls Parkway [39.31498 °N, 076.66565 °W]. Outcrop is mapped as belonging to the Druid Hill Amphibolite on the 1:24k Baltimore West quadrangle of the Maryland Geological Survey (Crowley & Reinhardt, 1979). At the location, amphibolites of the metavolcanic James Run Formation—of which the Druid Hill Amphibolite is the lowermost unit—host a heavily sheared felsic unit in addition to less-deformed, quartz metamicrodiorite (the rock sampled) that is interfingered with and surrounds the host (Fig. S1A). Crowley & Reinhardt (1979) mapped the unit as an effectively syn-magmatic phase of the Druid Hill Amphibolite, referring to it as "irregular anastomosing patches of coarser grained, lighter colored amphibolite". Field images of fresh Druid Hill Amphibolite host (left) and quartz metamicrodiorite sampled for MD19-22 (right) are in Fig. S1B.

In thin section, MD19-22 is ~45 modal% green amphibole, ~25 modal% saussuritised plagioclase and ~20 modal% quartz with foam texture microstructure, in addition to trace epidote and opaque minerals. Typical photomicrographs of MD19-22, in both plane and cross polarized light, are in Fig. S2.

PSB19-01: Quartz metagabbro sampled from outcrop at the south end of Conowingo Creek Landing, ~100 m upstream from where Conowingo Creek meets the Susquehanna River, close to the disused rail along the Susquehanna [39.68293 °N, 076.19543 °W]. Sample is from a ~4 km-wide, NE-striking metagabbroic body that, with ultramafic units, a large felsic body (the Port Deposit Tonalite) and metavolcanics of the James Run Formation (including pillow metabasalts at Gilpin Falls), forms the State Line Complex (see mapped units of Southwick, 1969). Photo of the outcrop from which PSB19-01 was sampled is in Fig. S1C.

In thin section, PSB19-01 is ~55 modal% completely saussuritised plagioclase (~30 modal% of which is formed of euhedral zoisite clusters), ~42 modal% hornblende, 1–2 modal% quartz and ~1 modal% white mica, with trace opaque minerals. Typical photomicrographs of PSB19-01, in both plane and cross polarized light, are in Fig. S2.

NL22-01: Plagiogranite sampled from exposed outcrop in heavily vegetated bogland of the Blow Me Down Mountain Massif, Newfoundland, at approximately 540 m above sea level and 2.7 km south of the sea, in the Bay of Islands area [49.04837 °N, 058.26951 °W]. Sample was taken from the same plagiogranite body as samples BMD-03-17Y, BMD-04-17Y, BMD-07-17Y, and BMD-08-17Y of Yan & Casey (2020), which is reported to occur within the upper gabbroic unit of the Bay of Islands Ophiolite Complex. Photo of the outcrop from which NL22-01 was sampled is in Fig. S1D. Exposed outcrop is felsic and contacts with surrounding gabbroic units could not be observed due to thick vegetation.

In thin section, NL22-01 is ~35 modal% quartz, ~45 modal% feldspar, ~10 modal% hornblende, ~8 modal% chlorite and ~2 modal% epidote group minerals, with trace garnet and opaque minerals. Typical photomicrographs of NL22-01, in both plane and cross polarized light, are in Fig. S2.

NL22-04: Plagiogranite sampled from within Blow Me Down Provincial Park at the neck of Tortoise Point Peninsula, between York Harbour and Lark Harbour, Newfoundland [49.09155 °N, 058.36467 °W]. Sample was taken from ~50 m NE of sample CC-BMDP1-17ERS of Yan & Casey (2022), within the same large plagiogranite body (of the Coastal Complex) as sample 83GD-02 of Jenner et al. (1991). Exposed outcrop is felsic and contacts with surrounding units could not be observed due to thick vegetation.

In thin section, NL22-01 is ~40 modal% quartz, ~45 modal% feldspar, ~10 modal% biotite and ~5 modal% hornblende, with trace epidote group minerals, garnet and opaque minerals. Typical photomicrographs of NL22-04, in both plane and cross polarized light, are in Fig. S2.

GH19-02: Mafic metagreywacke sampled from vegetated coastal hillside/cliff face mapped as "Bute Amphibolite" in Fig. 2B of Chew et al. (2010), immediately W of the northernmost, E–W trending coastline of Scalpsie Bay, Isle of Bute, SW Scotland [55.78078 °N, 005.10375 °W]. The outcrop is heavily overgrown, obscuring geological associations. The rock is grey–green mafic (hornblende–plagioclase) metagreywacke (Fig. S1E).

GH19-02 is heterogeneous, formed of domains that are ~60 modal% saussuritised feldspar, ~15 modal% hornblende, ~12 modal% quartz aggregations, ~10 modal% porphyroblastic zoisite and ~3 modal% titanite, and domains in which hornblende makes up ≥80 modal% of the rock and in which feldspar, quartz and calcite are also present. The rock is cut by thin quartz veins and cataclastic domains. Typical photomicrographs of GH19-02, in both plane and cross polarized light, are in Fig. S2.

UN18-05: Metagabbro sampled from the far-SW end of coastal outcrop to the SW of Uyeasound Harbour [60.68740 °N, 000.92016 °W]. Outcrop is mapped as belonging to the Lower Metagabbro of the Metagabbro Layer, Lower Nappe, Unst Ophiolite on the 1:50k Unst and Fetlar map of the British Geological Survey (British Geological Survey, 2002). Photo of the coastal outcrop from which UN18-05 was sampled is provided in Fig. S1F.

In thin section, UN18-05 is ~60 modal% hornblende, with ~42 modal% fine-grained, saussuritised plagioclase, ~3 modal% titanite with opaque mineral (ilmenite?) cores, and accessory matrix rutile. Typical photomicrographs of UN18-05, in both plane and cross polarized light, are in Fig. S2.

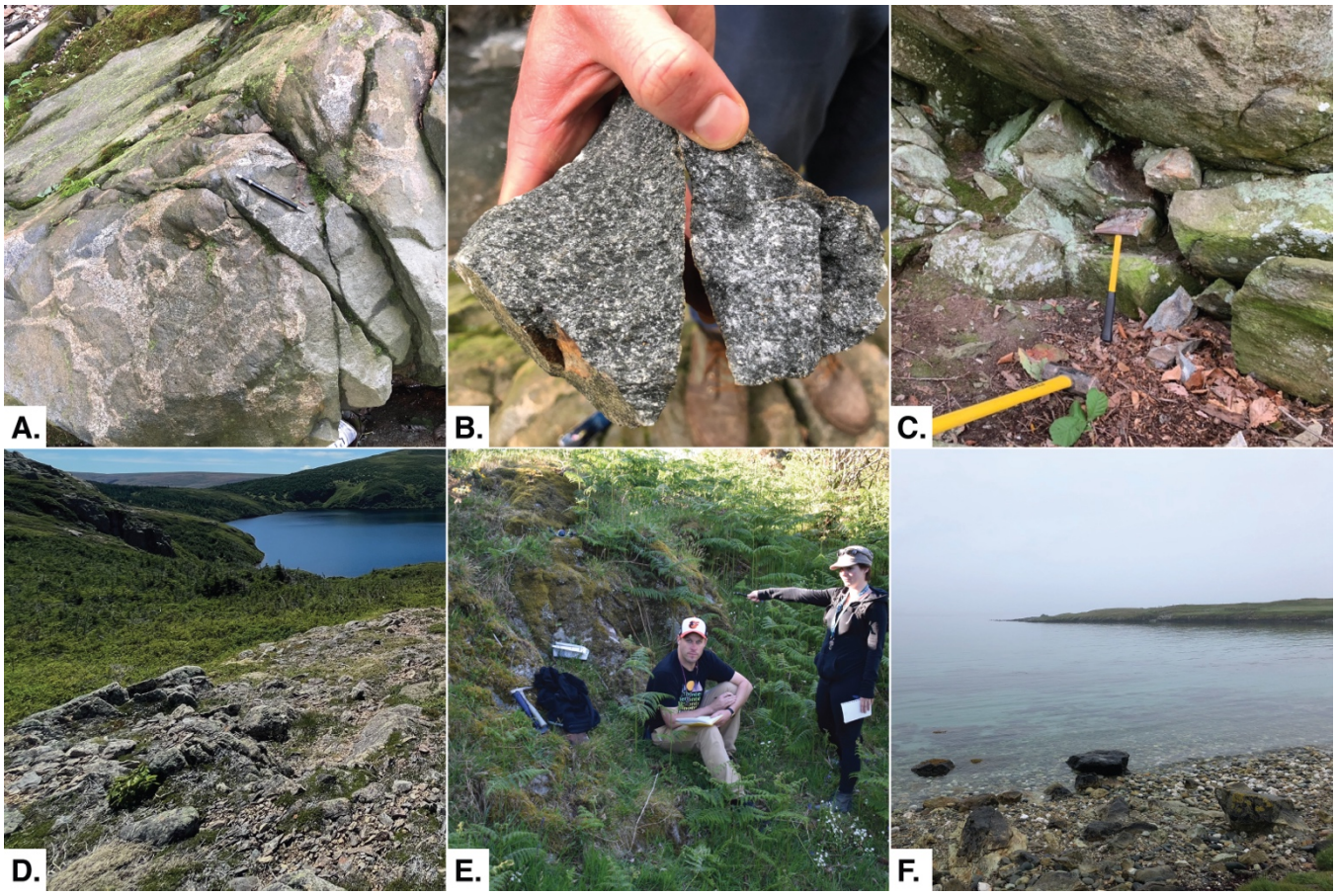

Figure S1. Selected field photos of rock samples of this study. (A) Outcrop from West Baltimore, showing brecciation textures in Druid Hill Amphibolite associated with metamicrodiorite sampled for MD19-22. (B) Field view of Druid Hill Amphibolite (left) and the metamicrodiorite sampled for MD19-22 (right). (C). Outcrop near to Conowingo Creek's outflow into the Susquehanna River, from which PSB19-01 was sampled. (D) Outcrop from Blow Me Down Mountain, Bay of Islands region, from which NL22-01 was sampled. (E) Vegetated hillside outcrop at location of mafic metagreywacke sample GH19-02 from Bute, SW Scotland. Sampling location for metagabbro sample UN18-05 on Uyeasound Harbour, Unst.

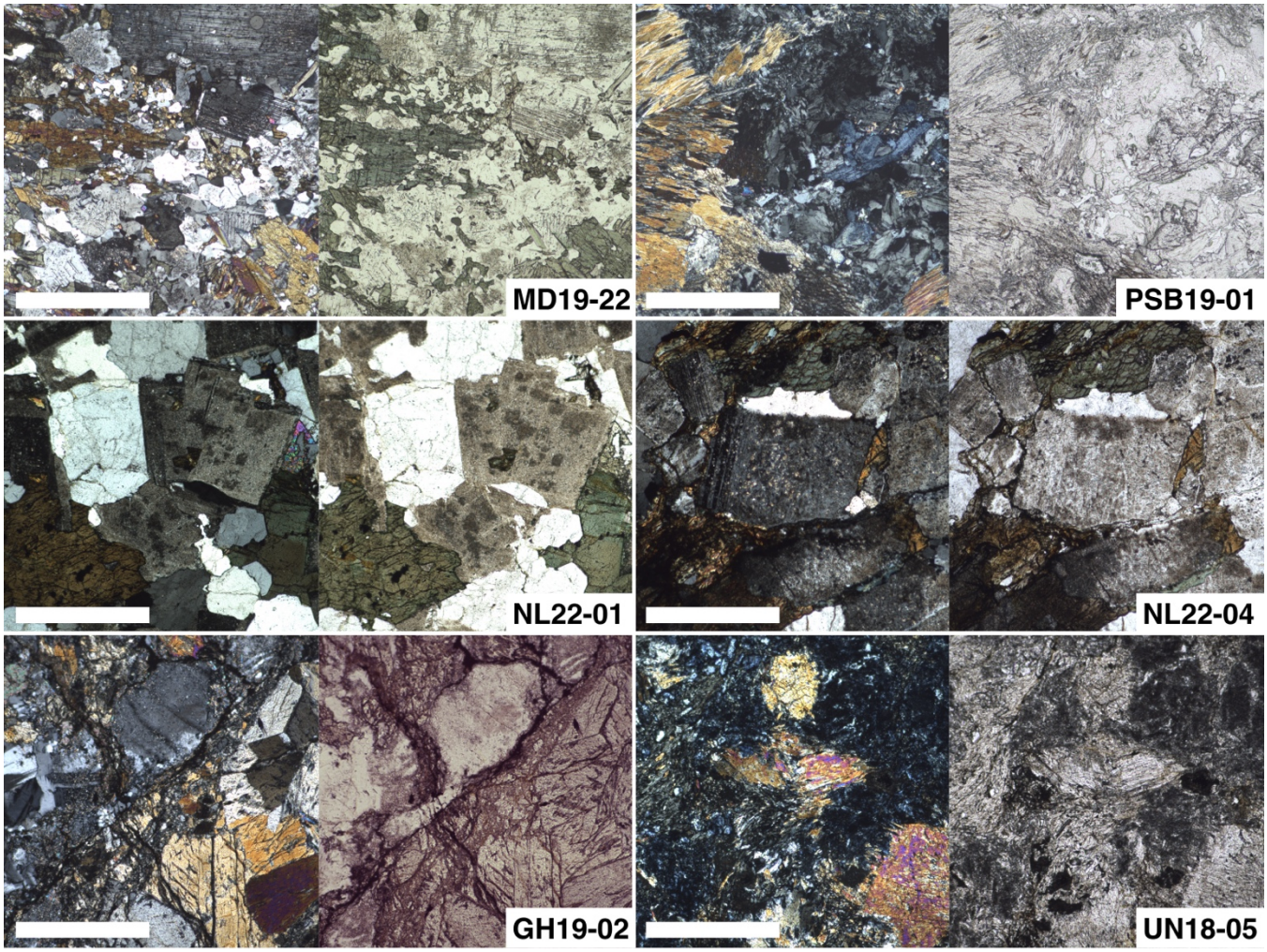

Figure S2. Photomicrographs of rock samples of this study. Cross- (left panel) and plane-polarised (right panel) images of the same field of view for each of the rocks studied. Sample number for each image pair is provided at the bottom left of the right (plane-polarised) image. White scale bar in cross-polarised light images is 1 mm in each case and is applicable also to the neighbouring plane-polarised light image.

S1.1.2. Cathodoluminescence images of zircons

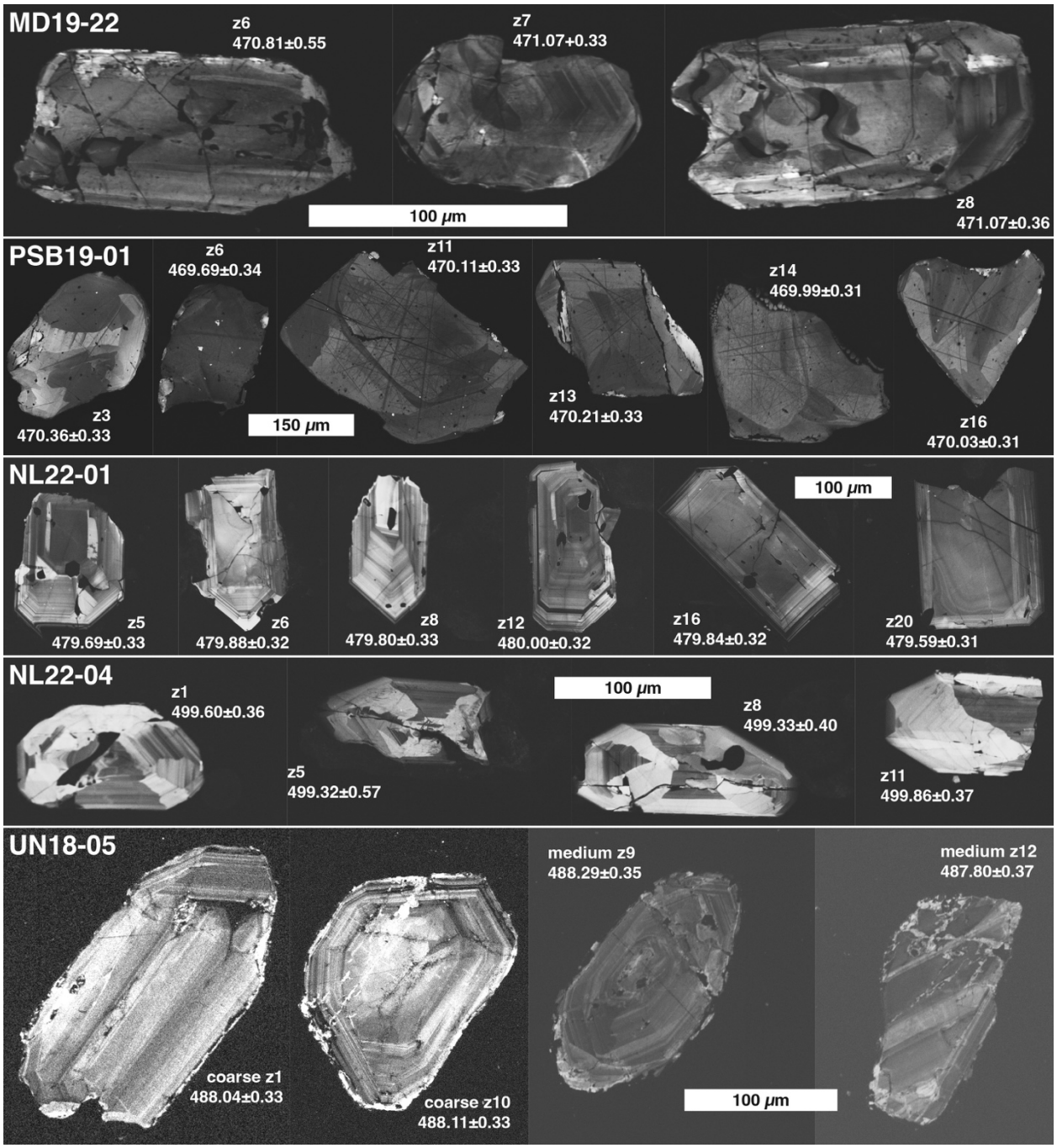

Figure S3. Cathodoluminescence (CL) images of all igneous zircons dated by chemical abrasion, isotope dilution thermal-ionization mass spectrometry (CA-ID-TIMS). Zircons from each sample are on separate rows, with relevant scale bar. Dates provided are single grain, $^{206}Pb/^{238}U$ estimates with 2σ uncertainty.

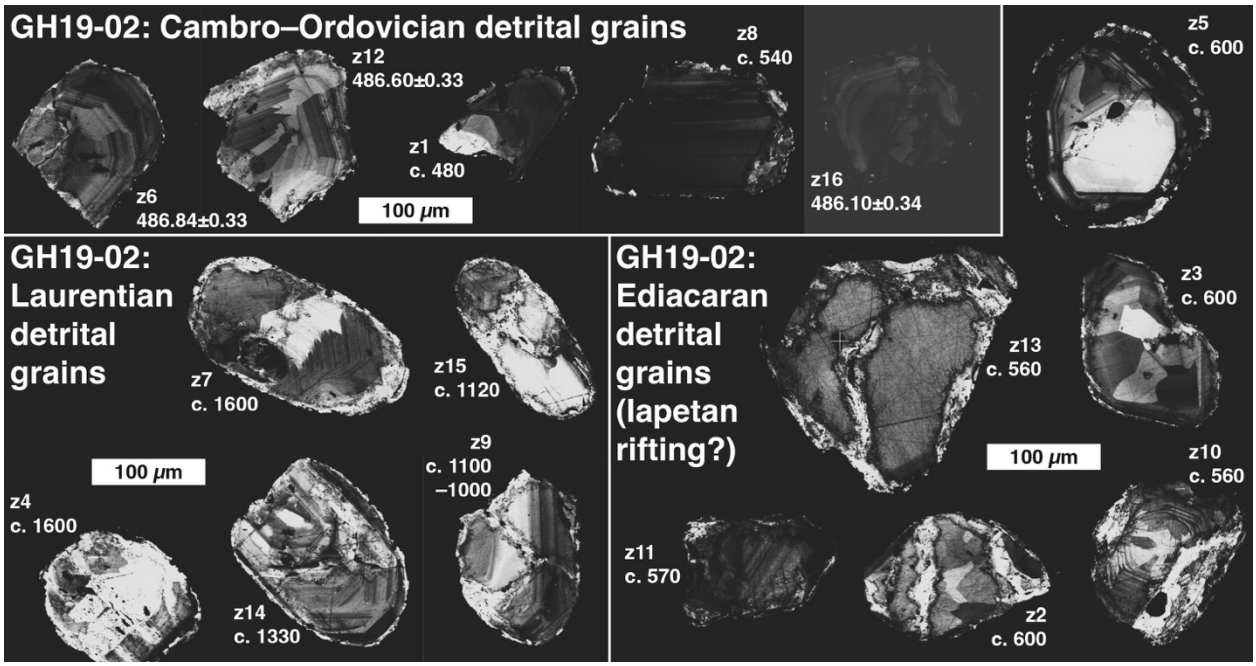

Figure S4. CL images of all dated detrital zircons from mafic greywacke GH19-02. Zircons are separated into three populations: (1) Cambro-Ordovician grains associated with the Highland Border Complex supra-subduction zone (SSZ) ophiolite; (2) Ediacaran grains associated with Iapetan rifting; (3) grains with ages >800 Ma and consistent with Laurentian provenance. $^{206}Pb/^{238}U$ age estimates (2σ uncertainties) are provided for the four grains from Group 1 that were dated by CA-ID-TIMS. All other grains have approximate laser ablation, inductively-coupled-plasma mass spectrometry (LA-ICP-MS) $^{206}Pb/^{238}U$ age estimates.

S1.2. Detailed Methods

S1.2.1. Along-strike distance measurement and sample position estimation

Along-strike distance measurement employed a "100 km ruler", meaning that measurement was made with a series of end-to-end straight-line increments of 100 km, each oriented to best fit its 100 km length of margin. Where rock locations occurred within a 100 km increment, the sub-ruler fraction of length was determined by orthogonal projection from the ruler to the sampling locality. The measurement line follows, as best as possible, the SE extent of the Laurentian margin (the contact with peri-Laurentian units). Annotated maps for North America, Ireland and Britain, and Scandinavia, each showing the along-strike measurement line (in bold pink), are in Supplementary Materials 4 (SM4). File size dictates that the maps provided in SM4 are relatively low-resolution; the original maps (as vector files) can be obtained from sources cited in the detailed text below.

For North America, distance was calculated from the 1:1,500,000 South and North Sheets of the Lithotectonic Map of the Appalachian Orogen, Canada–United States of America, compiled by Hibbard et al. (2003). The measurement line starts at the position of AL20-35, at the SW end of the Dadeville Complex, and moves along the Brevard Zone to the NE, to where the mapped shear zone ends at the Grandfather Mountain Window. From there, the measurement line continues to follow the same lithotectonic boundary as the Brevard Zone does, running along the SE boundary of the "Multiply tectonized accretionary complex" unit of the Piedmont Domain, through the Baltimore Mafic and State Line Complexes, to the end of the South Sheet at New York City. On the North Sheet, the measurement line follows the SE boundary of the "Iapetan rift and drift facies" units of the Laurentian Realm, through New England and the Mont Ham–

Thetford Mines Ophiolite of Quebec, to the end of the Gaspé Peninsula. From there it runs parallel with the trace of the "Appalachian Structural Front" through the Gulf of St Lawrence and along the Baie Verte–Brompton Line, past the Bay of Islands Ophiolite and Coastal Complexes and the Betts Cove Ophiolite through to Horse Islands, offshore of Biae Verte. The North American segment of the measurement line ends where the Newfoundland continental shelf ends, ~400 km offshore of Horse Islands. The North American segment of the measurement line (Dadeville Complex to the Newfoundland continental shelf) is 3,850 km in length.

For Ireland and Britain, distance was calculated from the 1:1,250,000 Bedrock Geology Map of the United Kingdom and Ireland (Holbrook et al., 2017). The Irish and British segment of the Caledonides was taken to begin at the continental shelf off of Western Ireland, ~350 km offshore of Slyne Head. From Slyne Head and the Connemara coastline, the measurement line tracks the terrane-bounding Fair Head–Clew Bay Line across the island of Ireland, running past Lough Nafooey, along the Belhavel Fault and Omagh Thrust then across the North Channel from Ireland to the Isle of Arran, Scotland. The measurement line follows the Highland Boundary Fault to the River Tay, where it then follows the Portsoy–Duchray Hill Lineament out to the NE coast of Scotland at Portsoy. It takes a 250 km direct line from Portsoy on the coast of the Scottish mainland to the southern end of the Shetland Archipelago, where it runs for another 105 km NNE, through the Unst Ophiolite, to the northernmost tip of Unst. The Ireland and Britain segment of the measurement line (Irish Continental Shelf to the top of Unst) is 1,400 km in length.

For Scandinavia, distance was calculated from the Tectonic Map of the Scandinavian Caledonides in Fig. 1 of Hollocher et al. (2012), which was made after the 1:2,000,000 Bedrock Map of Norway and the Caledonides of Sweden and Finland (Soli & Nordgullen, 2008). The Scandinavian segment of the Caledonides was taken to begin at Karmøy and the Karmøy Ophiolite in SW Norway, which is taken as an offset but equivalent position to the northern end of the Irish and British segment at Unst. The measurement line follows the Norwegian coastline past Bergen around to Kristiansund where it moves inland, following the contact between the peri-Laurentian Upper Allochthon and Laurentian Uppermost Allochthon. The line follows the Laurentian–peri-Laurentian contact past the Leka Ophiolite and Lyngen Magmatic Complex, ending at the coast beyond Tromsø in Arctic Norway. The Scandinavian segment of the measurement line is 1,500 km in length, for a total (Alabama to Arctic Norway) length of 6,750 km.

S1.2.2. Whole-rock geochemistry

S1.2.2.1. Major and minor element geochemistry by X-ray fluorescence spectroscopy

Samples were cut into ~2 cm pieces with a diamond saw and 40–100 g of mineralogically and texturally representative, rind- and vein-free material was selected for powdering. Powdering used a tungsten carbide ring-and-puck mill at Johns Hopkins University (JHU) and individual sample powders were sent to Franklin & Marshall College. Loss on ignition (LOI) values were calculated from mass loss following heating of 1 g of powder at 950 °C for 1.5 h. Glass disks were made by quenching a melt consisting of 0.4 g of whole-rock powder and 3.6 g of lithium tetraborate; flux melting was performed under an oxidising environment resulting in all Fe in the glass disk being Fe^{3+}. XRF values are reported for all major elements in manuscript Table 1.

Independent measurements of Fe^{3+}/Fe^{2+} were not made, but the major element concentration values used in the manuscript text, for the tectonomagmatic discrimination by the schemes of Shervais (1982) and Pearce & Reagan (2019) and in the plots of Fig. S5–S6, a $Fe^{3+}/(Fe^{3+}+Fe^{2+})$ value of 20% was assumed following the recommendations of Pearce & Reagan (2019) for SSZ ophiolite lithologies. X-ray fluorescence (XRF) spectroscopy measurements were performed using a Malvern Panalytical Zetium XRF vacuum spectrometer in the X-ray Laboratory, Franklin & Marshall College. Glass disks were returned to JHU for minor, trace and rare earth element analysis by inductively-coupled-plasma mass spectrometry (ICP-MS).

S1.2.2.2. Minor, trace and rare earth element geochemistry by laser ablation ICP-MS

Glass disks produced for XRF were shattered with a clean hammer, and small shards from each disk were mounted in epoxy to produce 1" mounts. Mounts were ground and polished to expose sufficient surface area for analysis of each shard. Multi-sample mounts were loaded into the HelEx II two-volume ablation cell of a Teledyne Cetac Analyte G2 laser ablation (LA) system connected to an Agilent 8900 triple quadrupole ICP-MS in the TeMPO Laboratory, JHU. Four or five of reference materials NIST610, NIST612 and USGS standards AGV-2G, BCR-2G and/or BHVO-2G were loaded with the unknowns. Whole-rock trace and rare earth element data were collected over four analytical sessions, on 18 July 2023 (NL22-04), 26 January 2024 (NL22-01), 15 January 2025 (GH19-02, UN18-05) and 5 September 2025 (MD19-22, PSB19-01).

LA-ICP-MS analysis was performed by LA raster lines, using a 50 µm square 'spot', repetition rate of 10 Hz, velocity of 10 µm s^{-1} and duration of 50–60 s, to produce a 500–600 µm line. A pre-ablation pass used a 60 µm square 'spot', repetition rate of 10 Hz and velocity of 100 µm s^{-1}. 25–40 s of washout time was allowed between LA raster lines. Analyses were performed at a laser fluence of 4.0 J cm^{-2}, with He flows of 0.5 L min^{-1} and 0.3 L min^{-1} into the ablation cell and cup, respectively. The He carrier gas (with analyte) was passed through a SQUID signal smoothing device then mixed with Ar make up gas at a rate of 0.9 L min^{-1} prior to injection into the ICP-MS. Analysis involved repeated, 3.761 s or 3.862 s sweeps of a set of 42 or 43 elemental masses, employing dwell times of 10 ms for ^{29}Si, 50 ms for ^{31}P, ^{43}Ca, ^{51}V, ^{52}Cr, ^{55}Mn, ^{59}Co, ^{60}Ni, ^{88}Sr and 100 ms for all others. Each unknown glass was analyzed in triplicate and values for each analyte were compared across the triplicate analyses to ensure consistency in results; reported values in manuscript Table 1 were taken as the median value of the triplicate analyses.

Data reduction was performed using iolite v.4 (Paton et al., 2011), with NIST612 used as the primary reference material (mean–median fit to the data) and ^{43}Ca as the internal standard (concentration taken from XRF analysis). Three or four of AGV-2G, BCR-2G, BHVO-2G and NIST610 were used as monitoring standards; their values (compared to Jochum et al., 2005) across all analytes listed with ppm elemental concentrations in manuscript Table 1 yielded a 2σ reproducibility of 11.7% for GH19-02 and UN18-05, 13.6% for MD19-22 and PSB19-01, 16.0% for NL22-01 and 9.9% for NL22-04. Full details of analytical settings, system and reference material performance for each analytical session are in SM2.

S1.2.3. Zircon U-Pb geochronology by LA-ICP-MS

Samples were cut into ~5–10 cm pieces with a diamond saw, jaw crushed and sieved to a >1 mm fraction. The >1 mm jaw crusher fraction was washed thoroughly to remove any fine material that had adhered to the chips, and thereby minimise likelihood of zircon contamination from the jaw crusher. Jaw crusher chips were crushed to <250 µm in a hardened steel ring-and-puck mill then sieved to <90 µm, 90–125 µm, 125–180 µm and 180–250 µm fractions. Sieved fractions were individually washed to remove clay- and silt-sized particles. Washed separates were subjected to magnetic separation using a S.G. Frantz LB-1 magnetic barrier separator then density separation using sodium polytungstate (specific gravity ≤3.05 g cm^{-3}) and/or diiodomethane (specific gravity of 3.32 g cm^{-3}), targeting highly non-magnetic and dense fractions likely to be enriched in zircon. Zircons were handpicked under reflected/transmitted light microscope and annealed in a muffle furnace at 900 °C for 60–66 h. Annealed zircons were mounted with grains of similar size, in epoxy, to produce 1" mounts. Mounts were ground and polished to expose zircon grains at their approximate midsection. All mineral separation and sample preparation work was performed at JHU.

Polished zircon mounts were carbon coated and grains were cathodoluminescence (CL) imaged using a Deben Centaurus CL detector on a Thermo Scientific Helios G5 UC focused ion beam–scanning electron microscope (FIB–SEM) in the Material Characterization & Processing (MCP) facility, JHU. Carbon coat was removed from mounts and they were loaded into the above-described LA system in the TeMPO Laboratory, JHU. Samples were analyzed by quadrupole LA-ICP-MS alongside zircon standards 91500 ($^{206}Pb/^{238}U$ age of 1063.6±0.3 Ma: Wiedenbeck et al., 1995; Schoene et al., 2006), FC-1 ($^{206}Pb/^{238}U$ age of

1099.9±1.1 Ma: Paces & Miller Jr, 1993), Plešovice ($^{206}Pb/^{238}U$ age of 337.13±0.37 Ma: Sláma et al., 2008) and Temora II ($^{206}Pb/^{238}U$ age of 416.78±0.33 Ma: Black et al., 2003). Zircon U-Pb geochronology was performed over five analytical sessions, on 27 August 2021 (UN18-05 coarse grains), 15 December 2021 (UN18-05 medium grains), 3 June 2022 (GH19-02), 22 November 2023 (MD19-22) and 17 January 2024 (NL22-01, NL22-04, PSB19-01). NIST612 was also analyzed during the 22 November 2023 and NIST610 and NIST612 during the 17 January 2024 session, in association with an expanded analytical approach (elemental geochemistry also considered) for unknown and reference material zircons (details below).

LA-ICP-MS analysis was performed using a 25, 30 or 40 µm square 'spot' (depending on zircon grain size), repetition rate of 8 or 10 Hz and total shot count of 200, 250 or 300. Analyses were performed at a laser fluence in the range 1.33–3.0 J cm^{-2}, with He flows into the ablation cell and cup, respectively, of 0.4 and 0.37 L min^{-1}, 0.71 and 0.35 L min^{-1}, 0.35 and 0.325 L min^{-1} or 0.5 and 0.3 L min^{-1}. The He carrier gas (with analyte) was passed through a SQUID signal smoothing device then mixed with Ar make up gas at a rate of 0.71 or 0.8 L min^{-1} prior to injection into the ICP-MS. Three cleaning shots then 20–30 s of washout time preceded each analysis. Analyses performed in 2021 or 2022 involved repeated, 1.0162 s mass sweeps, employing dwell times of 100 ms for ^{232}Th, ^{238}U and 200 ms for ^{204}Pb, ^{206}Pb, ^{207}Pb, ^{208}Pb. Analyses in 2023 and 2024 involved repeated, 1.1338 s mass sweeps, using the abovementioned dwell times for the Pb, Th and U isotopes, but also a 10 ms dwell time for each of ^{29}Si, ^{47}Ti, ^{88}Sr, ^{89}Y, ^{91}Zr, ^{93}Nb, ^{139}La, ^{140}Ce, ^{153}Eu, ^{157}Gd, ^{172}Yb, ^{175}Lu. All reference materials were analyzed once for every 3–10 unknown analyses. Details on exact analytical parameters used during each analytical session are in SM3.

Data reduction was performed in iolite v.4 (Paton et al., 2011) using the downhole fractionation correction routine of Paton et al. (2010) and 91500 as the primary reference material. Data reduction used a mean–median fit to the 91500 data, except for the session on 3 June 2022 that, due to significant, monotonic across-session drift, used a spline fit to the 91500 data. FC-1, Plešovice and Temora II were analyzed as secondary, tertiary and quaternary standards; for all standards from all five sessions, the $^{207}Pb/^{206}Pb$ and $^{206}Pb/^{238}U$ data yielded homogeneous age populations (expected MSWD for the n; see SM3 and Horstwood et al., 2016). Uncertainty on individual spot analyses (ellipses in Tera-Wasserburg plots) are given at 2s, where s is the internal analytical uncertainty calculated from repeated measurement of isotope abundance (counts). Uncertainty on weighted mean ages are reported in the form ± *X* | *Y*, where *X* considers only random uncertainties internal to the data (ignoring systematic uncertainties such as in the value of decay constants) and *Y* is the expanded uncertainty, 2s-sys, which includes a 2.5% excess uncertainty specific to the long-term accuracy of zircon reference materials dated in the TeMPO Laboratory, added in quadrature to the 2s value for the weighted mean age of the population (approach outlined in Horstwood et al., 2016).

Zircon U-Pb geochronology by LA-ICP-MS used the U isotopic composition of Hiess et al. (2012), and the ^{235}U–^{207}Pb and ^{238}U–^{206}Pb decay constants of Jaffey et al. (1971). Ratios from individual analyses (with 2s uncertainties), obtained following data reduction in iolitie v.4 (details above), were pasted into the online geochronology toolbox IsoplotR (Vermeesch, 2018), which was used for all data exploration, interpretation and visualisation.

S1.2.4. Zircon U-Pb geochronology by CA-ID-TIMS

U-Pb dates were obtained by the chemical abrasion isotope dilution thermal ionization mass spectrometry (CA-ID-TIMS) method from analyses composed of single zircon grains (Table 1), modified after Mattinson (2005). Zircon was removed from their epoxy mounts using CL images and LA-ICP-MS data to guide grain selection.

Zircon was loaded into 300 µL Teflon PFA microcapsules, placed in a large-capacity Parr vessel, and partially dissolved in 120 µL of 29 M HF for 12 h at 190 °C. Contents of the microcapsules were put in 3 mL Teflon PFA beakers, the HF was removed, and zircon was immersed in 3.5 M HNO_3, ultrasonically cleaned for 30 minutes, and fluxed on a hotplate at 80 °C for 1 h. The HNO_3 was removed and zircon was rinsed

twice in ultrapure H_2O before being reloaded into the 300 µL Teflon PFA microcapsules (rinsed and fluxed in 6 M HCl for several hours) and spiked with the Boise State University mixed ^{233}U-^{235}U-^{205}Pb tracer solution (BSU-1B). Zircon was dissolved in Parr vessels in 120 µL of 29 M HF at 220 °C for 48 h, dried to fluorides, and re-dissolved in 6 M HCl at 180 °C overnight. U and Pb were separated from the zircon matrix using an HCl-based anion-exchange chromatographic procedure (Krogh, 1973), eluted together and dried with 2 µl of 0.05 N H_3PO_4.

Pb and U were loaded on a single outgassed Re filament in 5 µL of a silica-gel/phosphoric acid mixture (Gerstenberger & Haase, 1997), and U and Pb isotopic measurements made on a GV Isoprobe-T multicollector TIMS equipped with an ion-counting Daly detector. Pb isotopes were measured by peak-jumping all isotopes on the Daly detector for 140–220 cycles, and corrected for 0.18 or 0.22 ± 0.03%/a.m.u. (1σ) mass fractionation. Transitory isobaric interferences due to high-molecular weight organics, particularly on ^{204}Pb and ^{207}Pb, disappeared within approximately 60 cycles. Linearity (to ≥1.4 x 10^6 cps) and the associated deadtime correction of the Daly detector were determined by analysis of NBS982. Uranium was analyzed as UO_2^+ ions in static Faraday mode on 10^{12} Ω resistors for 150–300 cycles, and corrected for isobaric interference of $^{233}U^{18}O^{16}O$ on $^{235}U^{16}O^{16}O$ with an $^{18}O/^{16}O$ of 0.00206. U mass fractionation was corrected using the known $^{233}U/^{235}U$ ratio of the BSU-1B tracer solution.

U-Pb dates and uncertainties were calculated using the algorithms of Schmitz & Schoene (2007), calibration of BSU-1B tracer solution of $^{235}U/^{205}Pb$ = 77.93, $^{233}U/^{235}U$ = 1.007066, and $^{205}Pb/^{204}Pb$ = 3491, U decay constants recommended by Jaffey et al. (1971), and $^{238}U/^{235}U$ = 137.818 (Hiess et al., 2012). $^{206}Pb/^{238}U$ ratios and dates were corrected for initial ^{230}Th disequilibrium using $D_{Th/U}$ = 0.20 ± 0.05 (1σ) and the algorithms of Crowley et al. (2007), resulting in an increase in the $^{206}Pb/^{238}U$ dates of ~0.09 Ma. All common Pb in analyses was attributed to laboratory blank and subtracted based on the measured laboratory Pb isotopic composition and associated uncertainty. U blanks are estimated at 0.013 pg.

Weighted mean $^{206}Pb/^{238}U$ dates were calculated from equivalent dates (probability of fit >0.05) using Isoplot 3.0 (Ludwig, 2003) with error at the 95% confidence interval. Error is computed as the internal standard deviation multiplied by the Student's t-distribution multiplier for a two-tailed 95% critical interval and n–1 degrees of freedom when the reduced chi-squared statistic, mean squared weighted deviation (MSWD; Wendt and Carl, 1991), takes a value less than its expected value plus its standard deviation at the same confidence interval, which is when MSWD is <1+2[2/(n–1)]^0.5. This error is expanded via multiplication by the MSWD^0.5 when the MSWD is ≥1+2[2/(n–1)]^0.5 to accommodate unknown sources of overdispersion. Errors on the weighted mean dates are given as ± *x* | *y* | *z*, where: *x* is the internal error based on analytical uncertainties only, including counting statistics, subtraction of tracer solution, and blank Pb subtraction; *y* includes the tracer calibration uncertainty propagated in quadrature; and *z* includes the ^{238}U decay constant uncertainty (Jaffey et al., 1971) propagated in quadrature. Internal errors should be considered when comparing our dates with $^{206}Pb/^{238}U$ dates from other laboratories that used the same tracer solution or a tracer solution that was cross calibrated using EARTHTIME gravimetric standards. Errors including the uncertainty in the tracer calibration should be considered when comparing our dates with those derived from other geochronological methods using the U-Pb decay scheme (e.g., LA-ICP-MS). Errors including uncertainties in the tracer calibration and ^{238}U decay constant should be considered when comparing our dates with those derived from other decay schemes (e.g., $^{40}Ar/^{39}Ar$, ^{147}Sm-^{143}Nd). Errors on dates from individual analyses are 2σ.

S1.3. Supporting Plots

S1.3.1. Whole-rock geochemistry and discrimination diagrams

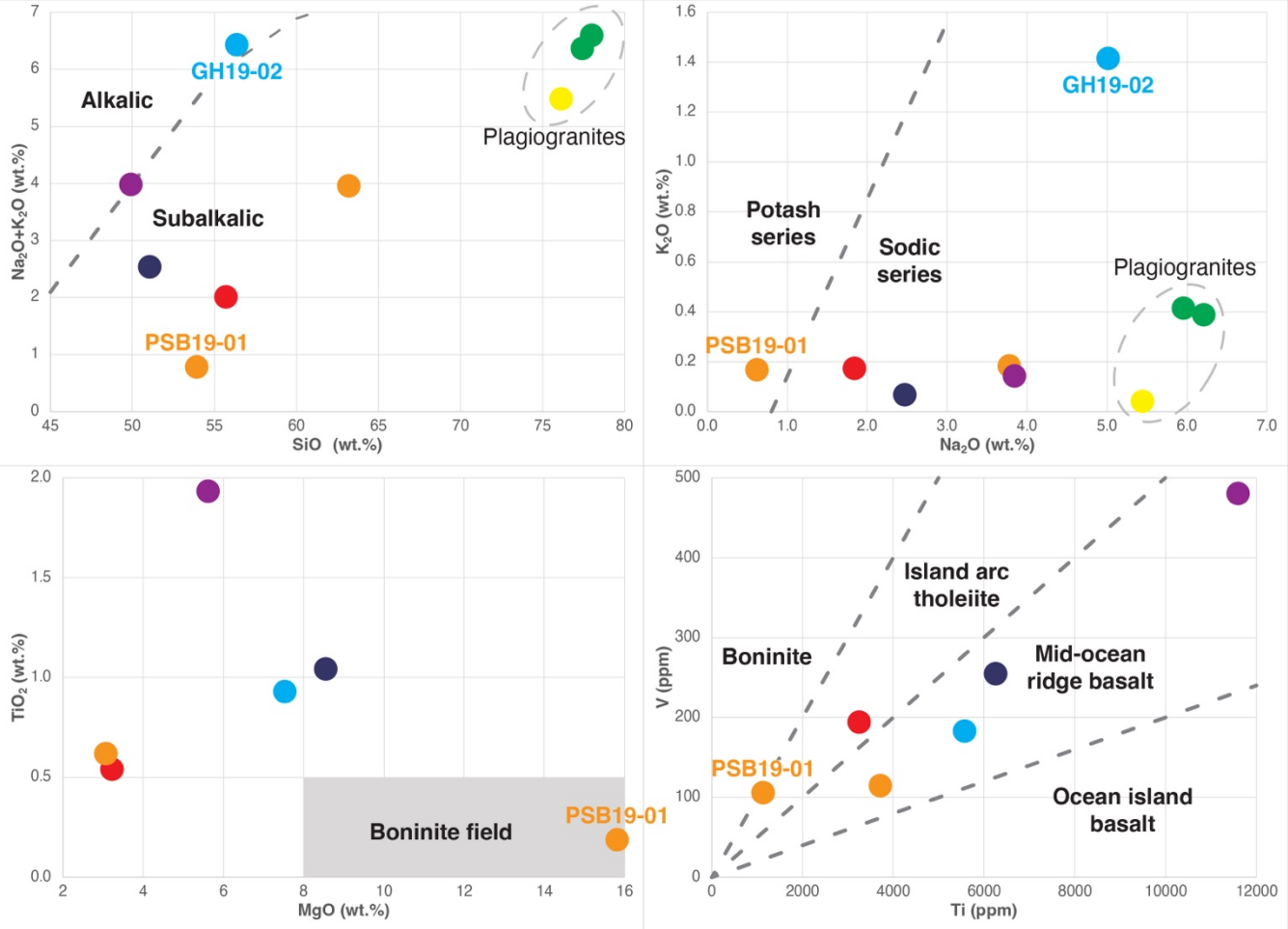

Figure S5. Major- and minor-element geochemistry of the rocks dated. Data coloured according to sample locations of manuscript Fig. 1; selected samples and sample groupings labelled. (A) Alkali v. SiO_2 plot of all rocks of this study with boundary of Alkalic and Sub-alkalic Series of Miyashiro (1978) shown. (B) K_2O v. SiO_2 plot of all rocks of this study with boundary of Potash and Sodic Series of Middlemost (1975). (C) TiO_2 v. MgO plot all mafic–intermediate rocks of this study with boninite field of Le Bas (2000) shown. (D) V v. Ti plot of all mafic–intermediate rocks of this study with SSZ ophiolite divisions of Shervais (1982) shown.

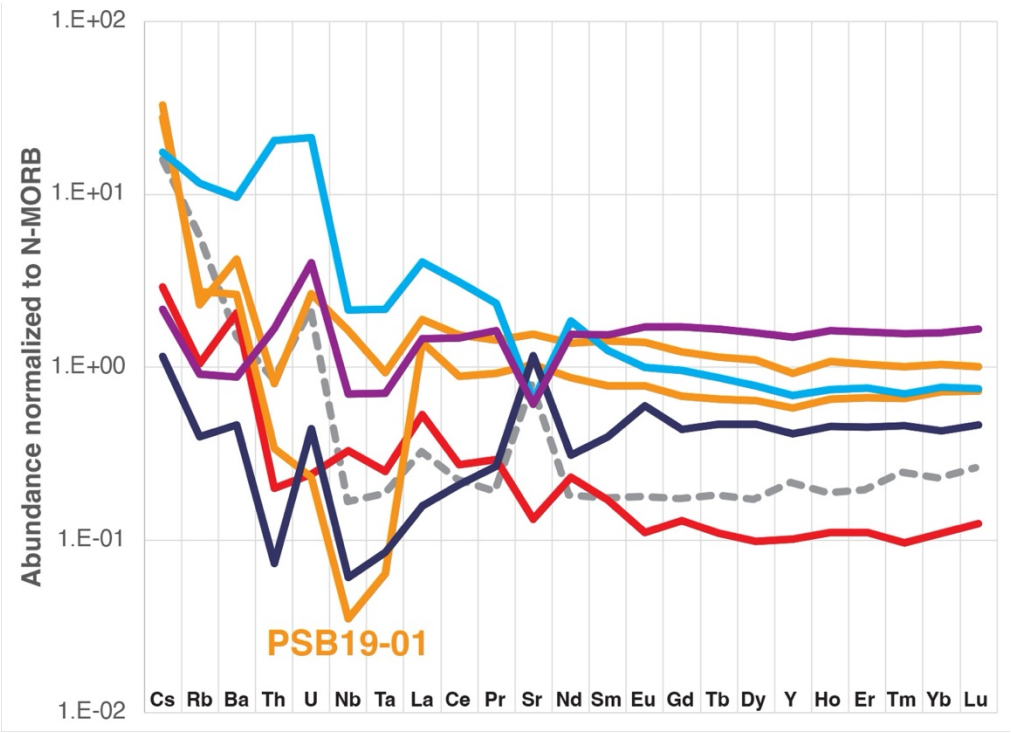

Figure S6. Trace and rare earth element geochemistry of the rocks dated. Extended spider plot, including the average boninite composition of Reagan et al. (2010) in grey, broken line. Elemental abundances normalized to normal mid-ocean ridge basalt values of Gale et al. (2013). Data colored according to sample locations of manuscript Fig. 1; selected samples labelled.

S1.3.2. Tera–Wasserburg and weighted mean plots for zircon U-Pb geochronology by LA-ICP-MS

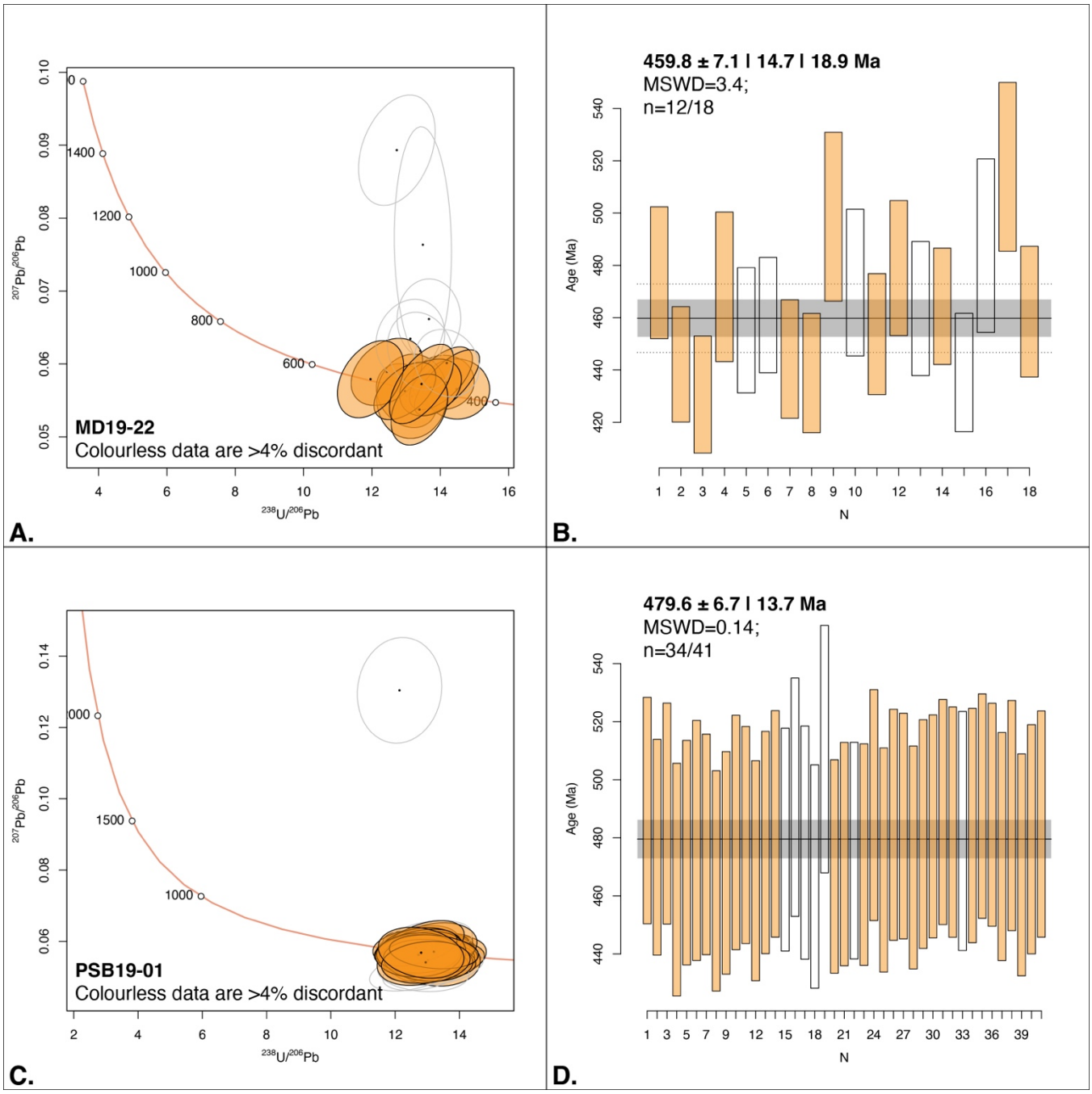

Figure S7. LA-ICP-MS geochronology of samples from Maryland, USA. Coloured data are concordant, having |1–($^{206}Pb/^{238}U$ date)/($^{207}Pb/^{235}U$ date)| <4%, shown with 2σ uncertainty. (A) Tera–Wasserburg plot and (B) $^{206}Pb/^{238}U$ weighted mean age plot for metamicrodiorite sample MD19-22 from the Baltimore Mafic Complex, with weighted mean date, MSWD and population details provided (note excessively-high MSWD for the sample size; uncertainties are 2s | 2s if individual analysis uncertainties are uniformly expanded to avoid overdispersion | 2s-sys). (C) Tera–Wasserburg plot and (D) $^{206}Pb/^{238}U$ weighted mean age plot for quartz metagabbro sample PSB19-01 from the State Line Complex, with weighted mean date (uncertainties are 2s | 2s-sys), MSWD and population details provided.

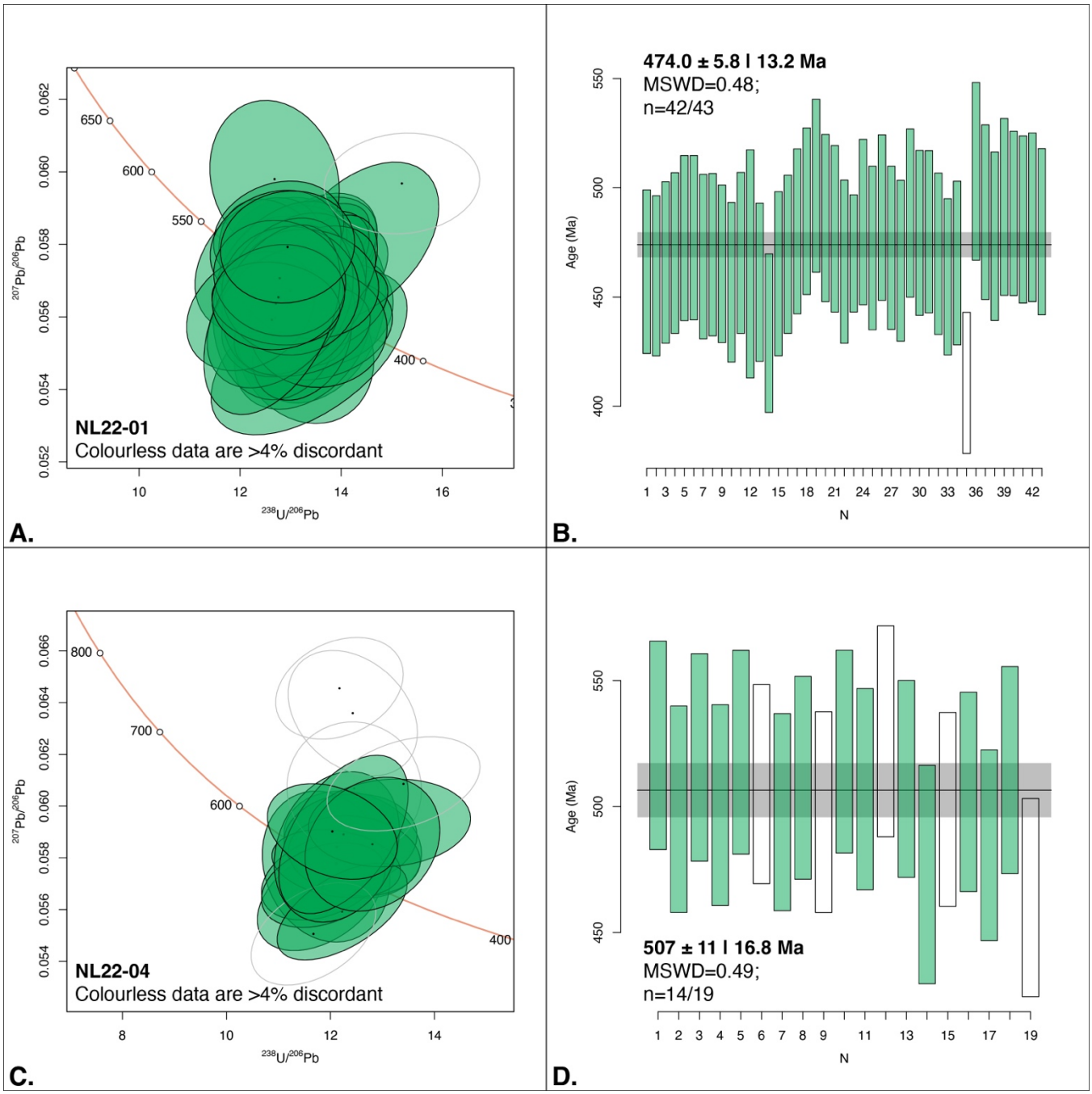

Figure S8. LA-ICP-MS geochronology for oceanic plagiogranite samples from western Newfoundland, Canada. Coloured data are concordant, having |1–($^{206}Pb/^{238}U$ date)/($^{207}Pb/^{235}U$ date)| <4%, shown with 2σ uncertainty. (A) Tera–Wasserburg plot and (B) $^{206}Pb/^{238}U$ weighted mean age plot for sample NL22-01 from the Bay of Islands Ophiolite Complex, with weighted mean date (uncertainties are 2s | 2s-sys), MSWD and population details provided. (C) Tera–Wasserburg plot and (D) $^{206}Pb/^{238}U$ weighted mean age plot for sample NL22-04 from the Coastal Complex, with weighted mean date (uncertainties are 2s | 2s-sys), MSWD and population details provided.

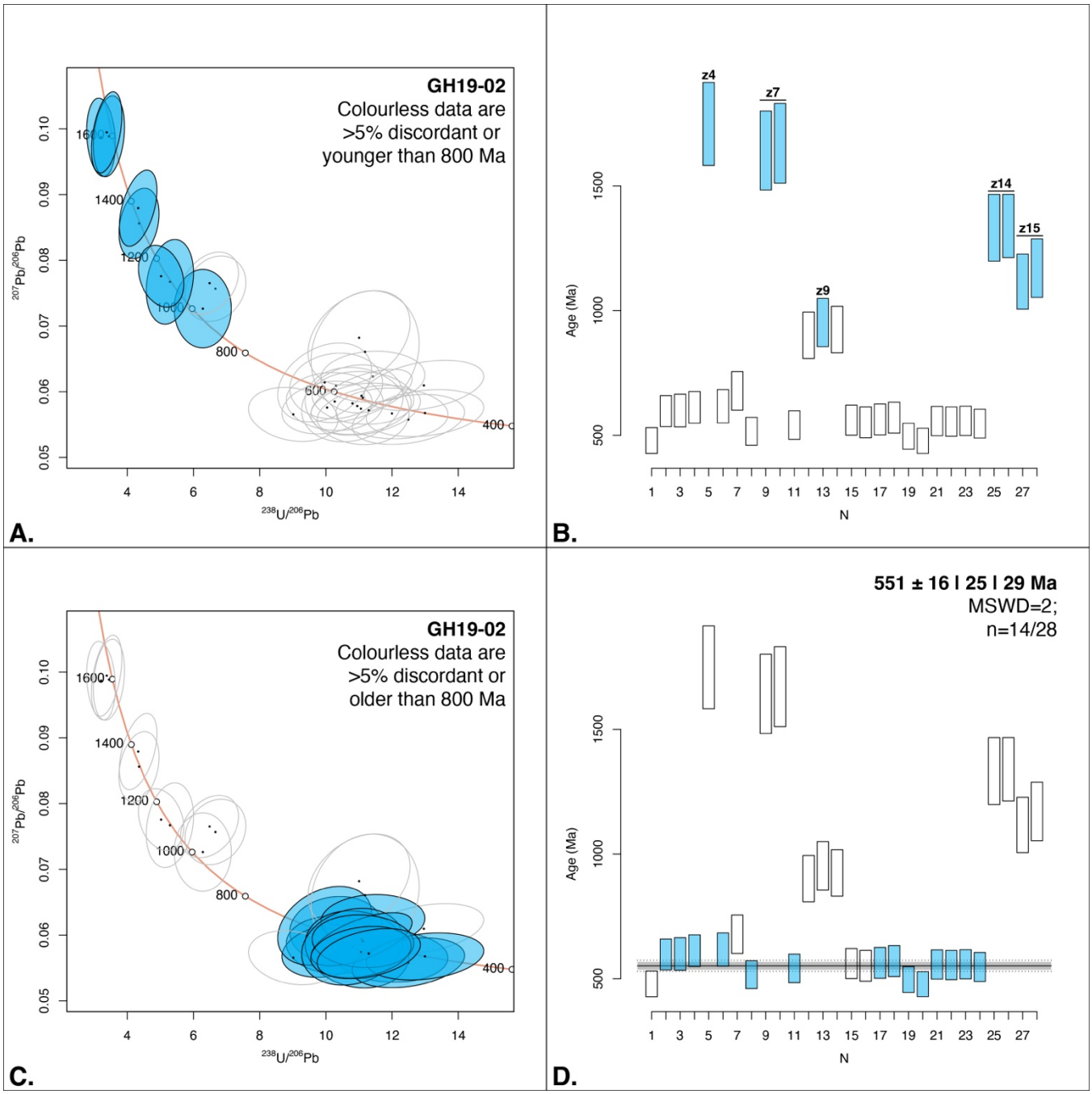

Figure S9. LA-ICP-MS geochronology for mafic metagreywacke sample GH19-02 from the Highland Border Complex at Bute, Scotland. Coloured data are concordant, having |1–($^{206}Pb/^{238}U$ date)/($^{207}Pb/^{235}U$ date)| <5%, shown with 2σ uncertainty. (A) Tera–Wasserburg plot and (B) $^{206}Pb/^{238}U$ weighted mean age plot for all zircons >800 Ma, with no weighted mean date calculated for the heterogeneous detrital population. (C) Tera–Wasserburg plot and (D) $^{206}Pb/^{238}U$ weighted mean age plot for all zircons <800 Ma, with weighted mean date, MSWD and population details provided (note excessively-high MSWD for the sample size; uncertainties are 2s | 2s if individual analysis uncertainties are uniformly expanded to avoid overdispersion | 2s-sys).

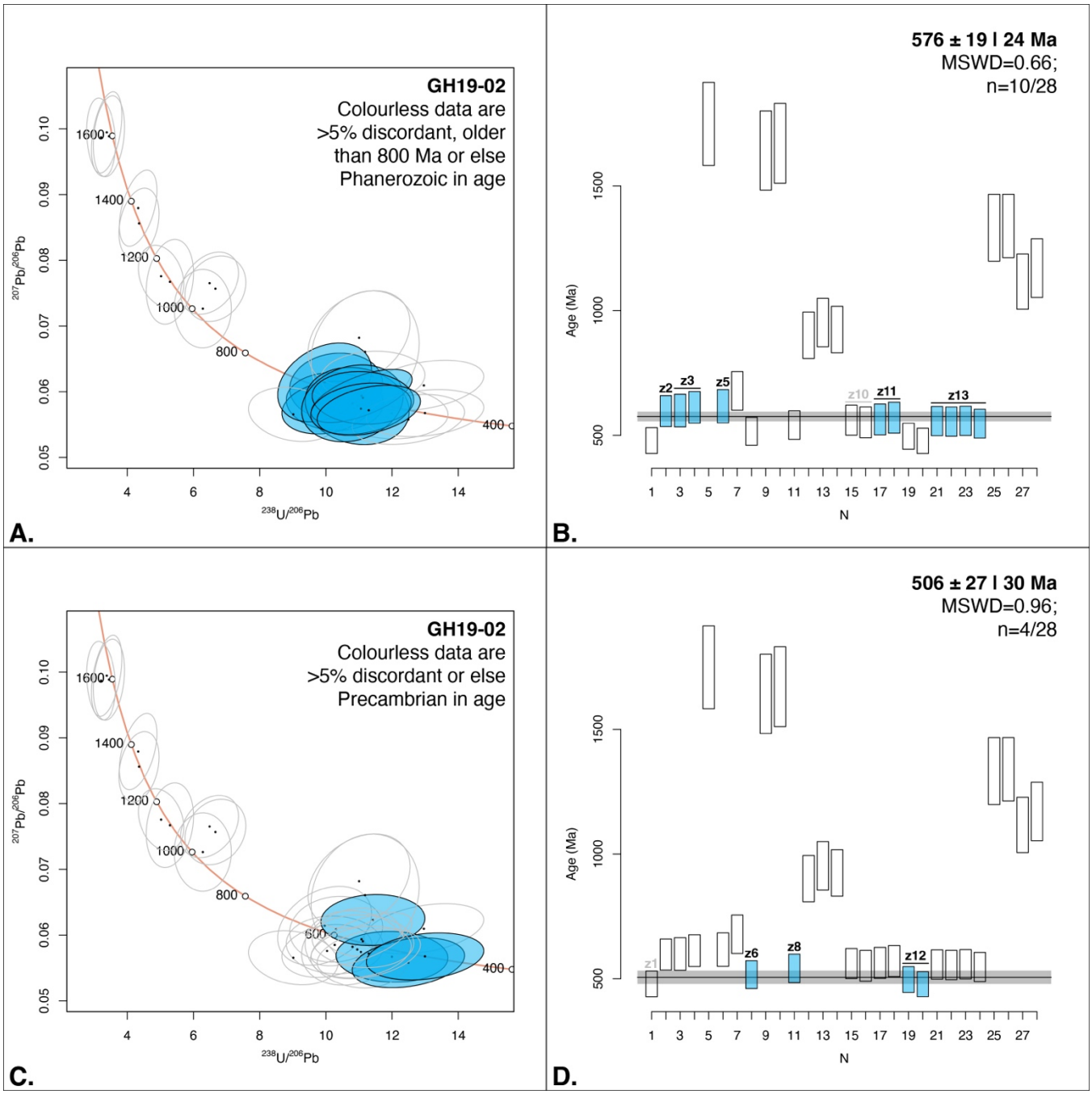

Figure S10. LA-ICP-MS geochronology of overdispersed, <800 Ma zircon population from mafic metagreywacke sample GH19-02 from the Highland Border Complex at Bute, Scotland. Coloured data are concordant, having |1–($^{206}Pb/^{238}U$ date)/($^{207}Pb/^{235}U$ date)| <5%, shown with 2σ uncertainty. (A) Tera–Wasserburg plot and (B) $^{206}Pb/^{238}U$ weighted mean age plot for all Ediacaran zircons, with weighted mean date (uncertainties are 2s | 2s-sys), MSWD and population details provided. (C) Tera–Wasserburg plot and (D) $^{206}Pb/^{238}U$ weighted mean age plot for all Phanerozoic zircons, with weighted mean date (uncertainties are 2s | 2s-sys), MSWD and population details provided.

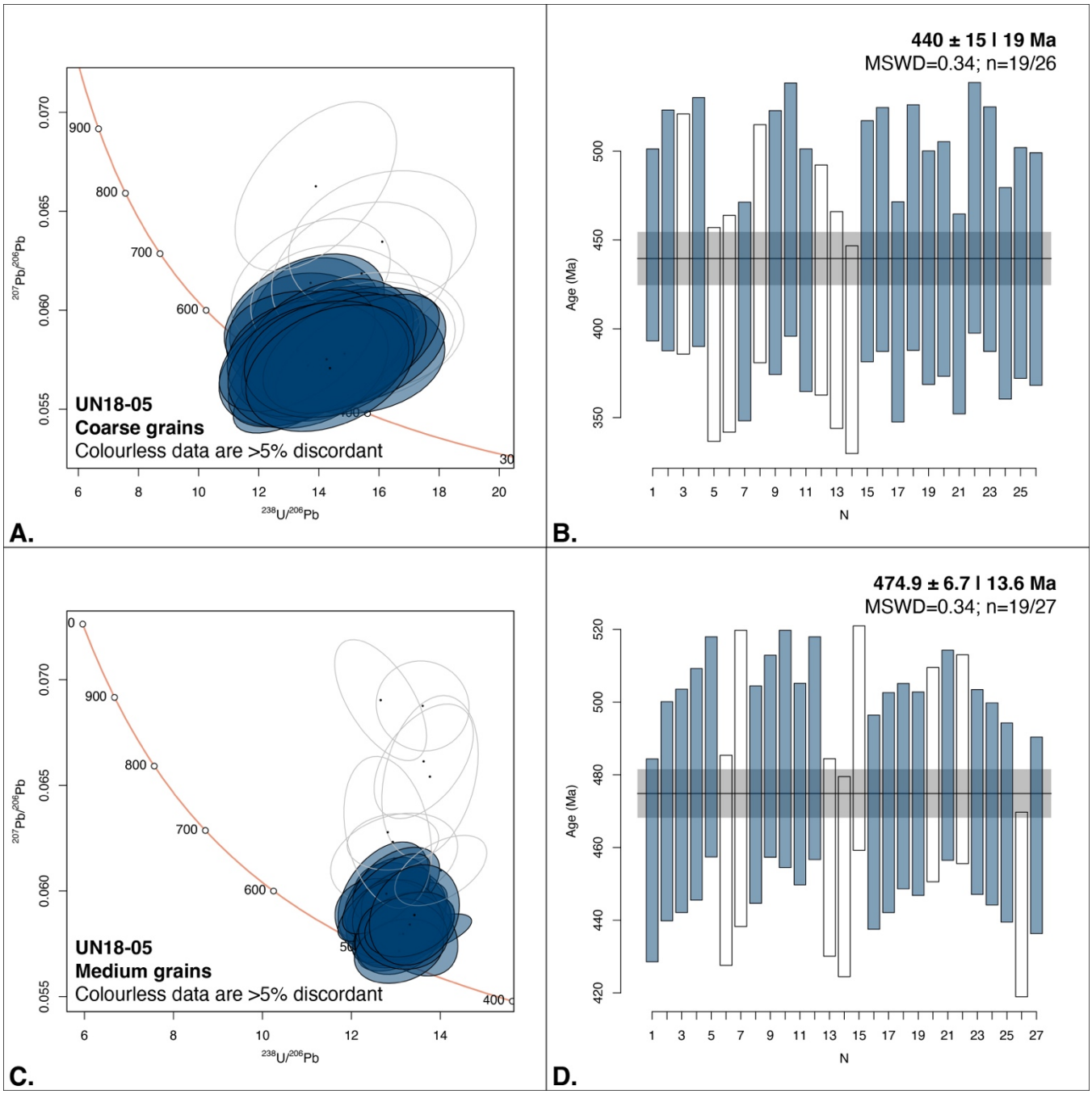

Figure S11. LA-ICP-MS geochronology of metagabbro sample UN18-05 from Unst, Shetland Archipelago, Scotland. Coloured data are concordant, having |1–($^{206}Pb/^{238}U$ date)/($^{207}Pb/^{235}U$ date)| <5%, shown with 2σ uncertainty. (A) Tera–Wasserburg plot and (B) $^{206}Pb/^{238}U$ weighted mean age plot for coarse zircon grains from UN18-05, with weighted mean date (uncertainties are 2s | 2s-sys), MSWD and population details provided. (C) Tera–Wasserburg plot and (D) $^{206}Pb/^{238}U$ weighted mean age plot for medium zircon grains from UN18-05, with weighted mean date (uncertainties are 2s | 2s-sys), MSWD and population details provided.

S1.4. References Cited

Black, L.P., Kamo, S.L., Allen, C.M., Davis, D.W., Aleinikoff, J.N., Valley, J.W., Mundil, R., Campbell, I.H., Korsch, R.J., Williams, I.S. & Poudoulis, C., 2004, Improved $^{206}Pb/^{238}U$ microprobe geochronology by the monitoring of a trace-element-related matrix effect; SHRIMP, ID-TIMS, ELA-ICP-MS and oxygen isotope documentation for a series of zircon standards. *Chemical Geology* **205**, 115–140.

British Geological Survey, 2002. Unst and Fetlar. Solid and Drift Geology. *Scotland 1:50,000 Map Series* **131**. British Geological Survey, Keyworth, Nottingham.

Chew, D.M., Daly, J.S., Magna, T., Page, L.M., Kirkland, C.L., Whitehouse, M.J. & Lam, R., 2010. Timing of ophiolite obduction in the Grampian Orogen. *Geological Society of America Bulletin* **122**, 1787–1799.

Crowley, J.L., Schoene, B. & Bowring, S.A., 2007. U-Pb dating of zircon in the Bishop Tuff at the millennial scale. *Geology* **35**, 1123–1126.

Crowley, W.P. & Reinhardt, J., 1979. Geological Map of the Baltimore West Quadrangle, Maryland. *1:24,000 Quadrangle Series*. Maryland Geological Survey, Baltimore, Maryland.

Gale, A., Dalton, C.A., Langmuir, C.H., Su, Y. & Schilling, J., 2013. The mean composition of ocean ridge basalts. *Geochemistry, Geophysics, Geosystems* **14**, 489–518.

Gerstenberger, H. & Haase, G., 1997. A highly effective emitter substance for mass spectrometric Pb isotope ratio determinations. *Chemical Geology* **136**, 309–312.

Hibbard, J.P., van Staal, C.R., Rankin, D.W. & Williams, H., 2003. Lithotectonic Map of the Appalachian Orogen, Canada–United States of America. *1:1,500,000 Scale Maps* **Map 2096A** (South and North Sheets). Geological Survey of Canada.

Hiess, J., Condon, D.J., McLean, N. & Noble, S.R., 2012. $^{238}U/^{235}U$ systematics in terrestrial uranium-bearing minerals. *Science* **335**, 1610–1614.

Holbrook, H., Barron, M., Krabbendam, M., Cooper, M. & Burke, H., 2017. Bedrock Geology of the United Kingdom and Ireland. *1:1,250,000 Scale Maps*. British Geological Survey.

Hollocher, K., Robinson, P., Walsh, E. & Roberts, D., 2012. Geochemistry of amphbolite-facies volcanics and gabbros of the Støren Nappe in extensions west and southwest of Trondheim, Western Gneiss Region, Norway: a key to correlations and paleotectonic settings. *American Journal of Science* **312**, 357–416.

Horstwood, M.S.A., Košler, J., Gehrels, G., Jackson, S.E., McLean, N., Paton, C., Pearson, N.J., Sircombe, K., Sylvester, P., Vermeesch, P., Bowring, J.F., Condon, D.J. & Schone, B., 2016. Community-derived standards for LA-ICP-MS (U-(Th-)Pb geochronology—uncertainty propagation, age interpretation and data reporting. *Geostandards & Geoanalytical Research* **40**, 311–332.

Jaffey, A.H., Flynn, K.F., Glendenin, L.E., Bentley, W.C. & Essling, A.M., 1971. Precision measurement of half-lives and specific activities of ^{235}U and ^{238}U. *Physical Review C* **4**, 1889–1906.

Jochum, K.P., Willbold, M., Raczek, I., Stoll, B. & Herwig, K., 2005. Chemical characterisation of the USGS reference glasses GSA-1G, GSC-1G, GSD-1G, GSE-1G, BCR-2G, BHVO-2G and BIR-1G using EPMA, ID-TIMS and LA-ICP-MS. *Geostandards & Geoanalytical Research* **3**, 285–302.

Krogh, T.E., 1973. A low contamination method for hydrothermal decomposition of zircon and extraction of U and Pb for isotopic age determination. *Geochimica et Cosmochimica Acta,* **37***,* 485–494.

Le Bas, M.J., 2000. IUGS reclassification of the high-Mg and picritic vocanic rocks. *Journal of Petrology* **41**, 1467–1470.

Ludwig, K.R., 2003. User's Manual for Isoplot 3.00. *Special Publication of the Berkeley Geochronology Center* **4**, pp. 74.

Mattinson, J.M., 2005. Zircon U-Pb chemical abrasion ("CA-TIMS") method: combined annealing and multi-step partial dissolution analysis for improved precision and accuracy of zircon ages. *Chemical Geology* **220***,* 47–66.

Middlemost, E.A.K., 1975. The basalt clan. *Earth Science Reviews* **11**, 337–364.

Miyashiro, A., 1978. Nature of alkalic volcanic rock series. *Contributions to Mineralogy & Petrology* **66**, 91–104.

Paces, J.B. & Miller Jr., J.D., 1993. Precise U-Pb ages of Duluth Complex and related mafic intrusions, Northeastern Minnesota: geochronological insights to physical, petrogenetic, paleomagnetic, and

tectonomagmatic processes associated with the 1.1 Ga Midcontinent Rift System. *Journal of Geophysical Research B* **98**, 13997–14013.

Paton, C., Woodhead, J.D., Hellstrom, J.C., Hergt, J.M., Greig, A., and Maas, R., 2010. Improved laser ablation U-Pb zircon geochronology through robust downhole fractionation correction. *Geochemistry, Geophysics, Geosystems* **11**, Q0AA06.

Paton, C., Hellstrom, J., Paul, B., Woodhead, J. & Hergt, J., 2011. Iolite: freeware for the visualisation and processing of mass spectrometric data. *Journal of Analytical Atomic Spectrometry* **26**, 2508–2518.

Reagan, M.K., Ishizuka, O., Stern, R.J., Kelley, K.A., Ohara, Y., Blichert-Toft, J., Bloomer, S.H., Cash, J., Fryer, P., Hanan, B.B., Hickey-Vargas, R., Ishii, T., Kimura, J.-I., Peate, D.W., Rowe, M.C. & Woods, M., 2010. Fore-arc basalts and subduction initiation in the Izu–Bonin–Marianas system. *Geochemistry Geophysics Geosystems* **11**, 3.

Schmitz, M.D. & Schoene, B., 2007. Derivation of isotope ratios, errors and error correlations for U-Pb geochronology using ^{205}Pb-^{235}U-(^{233}U)-spiked isotope dilution thermal ionization mass spectrometric data. *Geochemistry, Geophysics, Geosystems* **8**, Q08006.

Schoene, B., Crowley, J.L., Condon, D.J., Schmitz, M.D. & Bowring, S.A., 2006. Reassessing the uranium decay constants for geochronology using ID-TIMS U-Pb data. *Geochimica et Cosmochimica Acta* **70**, 426–445.

Shervais, J.W., 1982. Ti–V plots and the petrogenesis of modern and ophiolitic lavas. *Earth & Planetary Science Letters* **59**, 101–118.

Sláma, J., Košler, J., Condon, D.J., Crowley, J.L., Gerdes, A., Hanchar, J.M., Horstwood, M.S.A., Morris, G.A., Nasdala, L., Norberg, N., Schaltegger, U., Schoene, B., Tubrett, M.N. & Whitehouse, M.J., 2008. Plešovice zircon—A new natural reference material for U-Pb and Hf isotopic microanalysis. *Chemical Geology* **249**, 1–35.

Solli, A. & Nordgulen, Ø., 2008. Bedrock of Norway and the Caledonides in Sweden and Finland. *1:2,000,000 Scale Maps*. Geological Survey of Norway.

Southwick, D.L., 1969. *The Geology Harford County, Maryland*. Report of Investigation, Maryland Geological Survey.

Vermeesch, P., 2018. IsoplotR: a free and open toolbox for geochornology. *Geoscience Frontiers* **9**, 1479–1493.

Wendt, I. & Carl, C., 1991. The statistical distribution of the mean squared weighted deviation. *Chemical Geology* **86**, 275–285.

Wiedenbeck, M., Allé, P., Corfu, F., Griffin, W.L., Meier, M., Oberli, F., Von Quadt, A., Roddick, J.C. & Spiegel, W., 1995. Three natural zircon standards for U-Th-Pb, Lu-Hf, trace element and REE analyses. *Geostandards Newsletter* **19**, 1–23.

Yan, W. & Casey, J.F., 2020. A new concordia age for the 'forearc' Bay of Islands Ophiolite Complex, Western Newfoundland utilizing spatially-resolved LA-ICP-MS U-Pb analyses of zircon. *Gondwana Research* **86**, 1–22.